SCIENCE CHINA
Information Sciences

• RESEARCH PAPER •
Special Focus

March 2012 Vol. 55 No. 3: 501–511
doi: 10.1007/s11432-011-4531-1

Joint spatial registration and multi-target tracking using an extended PM-CPHD filter

LIAN Feng[1]*, HAN ChongZhao[1], LIU WeiFeng[2], LIU Jing[1] & YUAN XiangHui[1]

[1]*SKLMSE Lab, MOE KLINNS Lab, School of Electronics and Information Engineering, Xi'an Jiaotong University, Xi'an* 710049*, China;*
[2]*School of Automation, Hangzhou Dianzi University, Hangzhou* 310018*, China*

Received April 1, 2011; accepted November 24, 2011

Abstract An extended product multi-sensor cardinalized probability hypothesis density (PM-CPHD) filter for spatial registration and multi-target tracking (MTT) is proposed. The number and states of targets and the biases of sensors are jointly estimated by this method without the data association. Monte Carlo (MC) simulation results show that the proposed method (i) outperforms, although computationally more expensive than, the extended multi-sensor PHD filter which has been proposed for joint spatial registration and MTT; (ii) outperforms the multi-sensor joint probabilistic data association (MSJPDA) filter which is also extended in this study for joint spatial registration and MTT when the clutter is relatively dense.

Keywords multi-sensor spatial registration, multi-target tracking (MTT), cardinalized probability hypothesis density (PHD) filter, random finite set (RFS)

Citation Lian F, Han C Z, Liu W F, et al. Joint spatial registration and multi-target tracking using an extended PM-CPHD filter. Sci China Inf Sci, 2012, 55: 501–511, doi: 10.1007/s11432-011-4531-1

1 Introduction

Spatial registration (or alignment) is a prerequisite for the successful fusion of multiple sensors [1]. Many approaches have been proposed to solve the problem [2]. For most of the existing registration approaches, the association between targets and measurements must be known as a priori. However, the association is, in general, uncertain in the multi-target tracking (MTT) problems [3]. Therefore, how to align multiple sensors while performing MTT is still a very challenging topic.

A simple and intuitively natural solution for tackling the problem can be described as follows. At each time, the association relationship is first obtained via some classical association methods [4]. The measurements originating from the common targets are then provided for spatial registration and target state estimation according to the estimated association results. However, once the targets or clutter are relatively dense, the result of the data association would become rather bad due to the effect of sensor biases. The possibly incorrect association would then lead to the impairment of the spatial registration performance. As a consequence, the sensor bias estimates would diverge and the targets would be lost rapidly. Therefore, it is urgent to find a novel alternative method.

*Corresponding author (email: lianfeng1981@gmail.com)

Recently, the random finite set (RFS)-based tracking approaches, especially for the probability hypothesis density (PHD) [5] and cardinalized PHD (CPHD) [6] filters, have attracted extensive attention. Since the PHD and CPHD filters can avoid the complicated data association process, they are promising methods for the problem of joint spatial registration and tracking. However, the registration problem is rarely considered in the RFS-based approaches. Although an extended multi-sensor PHD filter for joint spatial registration and MTT has been proposed in 2011 [7], the approximation in the measurement-updated equation of the method is valid only for relatively large number of targets. When the number of targets is relatively small, the method might produce unsatisfactory results.

The product multi-sensor CPHD (PM-CPHD) filter, proposed by Mahler [8], is a middle ground between the 'true' but intractable multi-sensor CPHD filters and the tractable but heuristic iterated-corrector CPHD filters. This paper extends the standard PM-CPHD filter to accommodate the problem of spatial registration. Similar with the standard CPHD filter, the proposed PM-CPHD filter propagates not only the PHD but also the entire probability distribution on the target number. Consequently, compared with the extended multi-sensor PHD filter, more stable and accurate estimates of the multi-target number, multi-target states and sensor biases could be jointly derived from the proposed method.

Finally, we present two two-dimensional tracking examples, where multiple targets are tracked by three dissimilar but synchronous sensors. The observations received at the sensors are characterized by both the random noise and the translational measurement bias. In the first example, the proposed method is compared against the extended multi-sensor PHD filter. Monte Carlo (MC) simulation results show that the proposed method outperforms, although computationally more expensive than, the extended multi-sensor PHD filter. In the second example, the proposed approach is compared against the multi-sensor JPDA (MSJPDA) filter [9], which is also extended in this paper for joint spatial registration and MTT. The MC results show that the proposed method outperforms the MSJPDA filter when the clutter is relatively dense.

2 Background and problem formulation

At time k, let N_k denote the number of the existing targets, and $\boldsymbol{x}_k$ the state vector of a single target. Multi-target states can be represented as a finite set $X_k = \{\boldsymbol{x}_{k,n}\}_{n=1}^{N_k}$. We assume the system dynamics of the nth ($n = 1, \ldots, N_k$) existing target to be a Markov process with the transition density

$$f_{x,k|k-1}(\boldsymbol{x}_{k,n}|\boldsymbol{x}_{k-1,n}). \tag{1}$$

The targets are observed by S synchronous but biased sensors, where S is known a priori. Let M_k^j denote the number of the unlabeled measurements received at the jth ($j = 1, \ldots, S$) sensor, and $\boldsymbol{z}_k^j$ the single measurement vector. The measurements from the jth sensor can also be represented as a finite set $Z_k^j = \{\boldsymbol{z}_{k,m}^j\}_{m=1}^{M_k^j}$. All measurements at each time step are assumed to be independent [3]. Each measurement error is composed of independent identically distributed (i.i.d) random observation noise and sensor spatial biases (or systematic errors). Because of the effects of the measurement errors, the measurements generated by the common targets cannot superpose well when they are transformed from the local sensor coordinate system to a common coordinate system.

At time k, let $\boldsymbol{b}_k^j$ denote the bias vector of the jth sensor, and $\boldsymbol{b}_k = [(\boldsymbol{b}_k^1)^{\mathrm{T}}, \ldots, (\boldsymbol{b}_k^S)^{\mathrm{T}}]$ the S sensors' bias vector. We assume that the biases are independent, and the system dynamics of each bias is Markovian. Therefore, the transition density of $\boldsymbol{b}_k$ can be denoted by

$$f_{b,k|k-1}(\boldsymbol{b}_k|\boldsymbol{b}_{k-1}) = f_{b,k|k-1}^1(\boldsymbol{b}_k^1|\boldsymbol{b}_{k-1}^1) \cdots f_{b,k|k-1}^S(\boldsymbol{b}_k^S|\boldsymbol{b}_{k-1}^S), \tag{2}$$

where $f_{b,k|k-1}^j(\boldsymbol{b}_k^j|\boldsymbol{b}_{k-1}^j)$ is the transition density of the jth sensor's bias.

The measurement originates from either target or random clutter. If the mth measurement of the jth sensor $\boldsymbol{z}_{k,m}^j$ is generated by the nth target, then the likelihood for the biased measurement is denoted by

$$L_{\boldsymbol{z}_{k,m}^j}^j(\boldsymbol{x}_{k,n}, \boldsymbol{b}_k^j) = f_{k|k}^j(\boldsymbol{z}_{k,m}^j|\boldsymbol{x}_{k,n}, \boldsymbol{b}_k^j). \tag{3}$$

At time k, the jth sensor collects clutter (false alarms) with its spatial distribution given by the probability density $c_k^j(\boldsymbol{z}_k^j)$ and cardinality distribution given by $\kappa_k^j(m)$.

Let $Z_k^{1:S} = \{Z_k^1, \ldots, Z_k^S\}$ denote the set of the measurements received by all sensors at time k, and $Z_{1:k}^{1:S} = Z_1^{1:S}, \ldots, Z_k^{1:S}$ the measurement sequences up to time k. Given $Z_{1:k}^{1:S}$ and some prior information about the targets and the sensors, the objective of our paper is to estimate the sensors' bias $\boldsymbol{b}_k$, the number of the targets N_k, and the set of multi-target states $X_k = \{\boldsymbol{x}_{k,n}\}_{n=1}^{N_k}$.

3 Extended PM-CPHD filter

In order to derive the extended PM-CPHD filter for joint spatial registration and MTT, we first treat $(\boldsymbol{x}_k, \boldsymbol{b}_k)$ as an augmented state at time k. Analogous to the standard CPHD filter, let $\gamma_k(\boldsymbol{x}_k, \boldsymbol{b}_k)$ denote the PHD of the new birth augmented state. Assume that $\boldsymbol{b}_k$ is independent of $\boldsymbol{x}_k$. Then, the birth PHD, the transition density and the survival probability of the augmented state are, respectively, written as

$$\gamma_k(\boldsymbol{x}_k, \boldsymbol{b}_k) = \gamma_k(\boldsymbol{x}_k) + \gamma_k(\boldsymbol{b}_k), \tag{4}$$

$$f_{k|k-1}(\boldsymbol{x}_k, \boldsymbol{b}_k|\boldsymbol{x}_{k-1}, \boldsymbol{b}_{k-1}) = f_{x,k|k-1}(\boldsymbol{x}_k|\boldsymbol{x}_{k-1}) f_{b,k|k-1}(\boldsymbol{b}_k|\boldsymbol{b}_{k-1}), \tag{5}$$

$$p_{S,k|k-1}(\boldsymbol{x}_{k-1}, \boldsymbol{b}_{k-1}) = p_{S,k|k-1}(\boldsymbol{x}_{k-1}) p_{S,k|k-1}(\boldsymbol{b}_{k-1}). \tag{6}$$

Differently from the target number, the number of sensor biases is non-random and known as a priori. Therefore,

$$\gamma_k(\boldsymbol{b}_k) = 0; \quad p_{S,k|k-1}(\boldsymbol{b}_{k-1}) = 1. \tag{7}$$

At time k, let $D_{k|k-1}^{1:S}(\boldsymbol{x}_k, \boldsymbol{b}_k|Z_{1:k-1}^{1:S})$ and $D_{k|k}^{1:S}(\boldsymbol{x}_k, \boldsymbol{b}_k|Z_{1:k}^{1:S})$, respectively, denote the time-updated and measurement-updated PHDs of the augmented state from all sensors, hereafter abbreviated as $D_{k|k-1}^{1:S}(\boldsymbol{x}_k, \boldsymbol{b}_k)$ and $D_{k|k}^{1:S}(\boldsymbol{x}_k, \boldsymbol{b}_k)$; let $s_{k|k-1}^{1:S}(\boldsymbol{x}_k, \boldsymbol{b}_k|Z_{1:k-1}^{1:S})$ and $s_{k|k}^{1:S}(\boldsymbol{x}_k, \boldsymbol{b}_k|Z_{1:k}^{1:S})$, respectively, denote the time-updated and measurement-updated probability densities for the physical distribution of the augmented state from all sensors, hereafter abbreviated as $s_{k|k-1}^{1:S}(\boldsymbol{x}_k, \boldsymbol{b}_k)$ and $s_{k|k}^{1:S}(\boldsymbol{x}_k, \boldsymbol{b}_k)$.

$$s_{k|k-1}^{1:S}(\boldsymbol{x}_k, \boldsymbol{b}_k) = \frac{D_{k|k-1}^{1:S}(\boldsymbol{x}_k, \boldsymbol{b}_k)}{\int D_{k|k-1}^{1:S}(\boldsymbol{x}_k, \boldsymbol{b}_k) d\boldsymbol{x}_k d\boldsymbol{b}_k}; \quad s_{k|k}^{1:S}(\boldsymbol{x}_k, \boldsymbol{b}_k) = \frac{D_{k|k}^{1:S}(\boldsymbol{x}_k, \boldsymbol{b}_k)}{\int D_{k|k}^{1:S}(\boldsymbol{x}_k, \boldsymbol{b}_k) d\boldsymbol{x}_k d\boldsymbol{b}_k}. \tag{8}$$

Let $p_{k|k-1}^{1:S}(n|Z_{1:k-1}^{1:S})$ and $p_{k|k}^{1:S}(n|Z_{1:k}^{1:S})$, respectively, denote the probability distributions on the time-updated and measurement-updated target number from all sensors, hereafter abbreviated as $p_{k|k-1}^{1:S}(n)$ and $p_{k|k}^{1:S}(n)$; let $G_{k|k-1}^{1:S}(x)$, $G_{k|k}^{1:S}(x)$ and $C_k^j(z)$, respectively, denote the probability generating functions (PGFs) of $p_{k|k-1}^{1:S}(n)$, $p_{k|k}^{1:S}(n)$ and $\kappa_k^j(m)$.

$$\begin{aligned} G_{k|k-1}^{1:S}(x) &= \sum_{n=0}^{\infty} p_{k|k-1}^{1:S}(n) x^n; G_{k|k}^{1:S}(x) = \sum_{n=0}^{\infty} p_{k|k}^{1:S}(n) x^n; C_k^j(z) \\ &= \sum_{m=0}^{\infty} \kappa_k^j(m) z^m; (0 \leqslant x \leqslant 1; 0 \leqslant z \leqslant 1). \end{aligned} \tag{9}$$

The recursion of the extended PM-CPHD filter is given as follows.

The time-updated step is

$$\begin{aligned} D_{k|k-1}^{1:S}(\boldsymbol{x}_k, \boldsymbol{b}_k) &= \gamma_k(\boldsymbol{x}_k) \\ &+ \int p_{S,k|k-1}(\boldsymbol{x}_{k-1}) f_{x,k|k-1}(\boldsymbol{x}_k|\boldsymbol{x}_{k-1}) f_{b,k|k-1}(\boldsymbol{b}_k|\boldsymbol{b}_{k-1}) D_{k-1|k-1}^{1:S}(\boldsymbol{x}_{k-1}, \boldsymbol{b}_{k-1}) \mathrm{d}\boldsymbol{x}_{k-1} \mathrm{d}\boldsymbol{b}_{k-1}, \end{aligned} \tag{10}$$

$$p_{k|k-1}^{1:S}(n) \cong \sum_{i=0}^{n} p_B(n-i) \frac{1}{i!} (G_{k-1|k-1}^{1:S})^{(i)} (1 - s_{k-1|k-1}^{1:S}[p_{S,k|k-1}]) s_{k-1|k-1}^{1:S}[p_{S,k|k-1}]^i, \tag{11}$$

where

$$s^{1:S}[h] = \int h(\boldsymbol{x}, \boldsymbol{b}) s^{1:S}(\boldsymbol{x}, \boldsymbol{b}) \mathrm{d}\boldsymbol{x} \mathrm{d}\boldsymbol{b}, \tag{12}$$

and $p_B(n)$ is the probability distribution on birth target number.

Assuming that the clutter and predicted multi-target processes are i.i.d cluster processes [6] and the sensors are independent, the measurement-updated step is

$$D^{1:S}_{k|k}(\boldsymbol{x}_k, \boldsymbol{b}_k) = \frac{\hat{G}^{(1)}(\sigma)}{\hat{G}(\sigma)} \frac{L^1_{Z^1_k}(\boldsymbol{x}_k, \boldsymbol{b}_k) \cdots L^S_{Z^S_k}(\boldsymbol{x}_k, \boldsymbol{b}_k)}{N^1_{k|k} \cdots N^S_{k|k}} s^{1:S}_{k|k-1}(\boldsymbol{x}_k, \boldsymbol{b}_k), \tag{13}$$

$$p^{1:S}_{k|k}(n) = \frac{l^1_{Z^1_k}(n) \cdots l^S_{Z^S_k}(n) \sigma^n}{\hat{G}(\sigma)} p^{1:S}_{k|k-1}(n), \tag{14}$$

where

$$\sigma = \frac{s^{1:S}_{k|k-1}[L^1_{Z^1_k} \cdots L^S_{Z^S_k}]}{N^1_{k|k} \cdots N^S_{k|k}}; \quad \hat{G}(x) = \sum_{n=0}^{\infty} l^1_{Z^1_k}(n) \cdots l^S_{Z^S_k}(n) p^{1:S}_{k|k-1}(n) x^n, \tag{15}$$

and for $j = 1, \ldots, S$,

$$l^j_{Z^j_k}(n) = \sum_{i=0}^{\min\{n, M^j\}} (C^j_k)^{(M^j - i)}(0) i! C_{n,i} s^{1:S}_{k|k-1}[1 - p^j_D]^{n-i} \sigma^j_i(Z^j_k), \tag{16}$$

$$L^j_{Z^j_k}(\boldsymbol{x}, \boldsymbol{b}) = \alpha^j_0 (1 - p^j_D(\boldsymbol{x}, \boldsymbol{b})) + \sum_{\boldsymbol{z}^j \in Z^j_k} \frac{p^j_D(\boldsymbol{x}, \boldsymbol{b}) L^j_{\boldsymbol{z}^j}(\boldsymbol{x}, \boldsymbol{b}) \alpha^j(\boldsymbol{z}^j)}{c^j_k(\boldsymbol{z}^j)}, \tag{17}$$

$$N^j_{k|k} = \alpha^j_0 s^{1:S}_{k|k-1}[1 - p^j_D] + \sum_{\boldsymbol{z}^j \in Z^j_k} \frac{s^{1:S}_{k|k-1}[p^j_D L^j_{\boldsymbol{z}^j}] \alpha^j(\boldsymbol{z}^j)}{c^j_k(\boldsymbol{z}^j)}, \tag{18}$$

$$\alpha^j_0 = \frac{\sum_{l=0}^{M^j} (C^j_k)^{(M^j - l)}(0) (G^{1:S}_{k|k-1})^{(l+1)} (s^{1:S}_{k|k-1}[1 - p^j_D]) \sigma^j_l(Z^j_k)}{\sum_{i=0}^{M^j} (C^j_k)^{(M^j - i)}(0) (G^{1:S}_{k|k-1})^{(i)} (s^{1:S}_{k|k-1}[1 - p^j_D]) \sigma^j_i(Z^j_k)}, \tag{19}$$

$$\alpha^j(\boldsymbol{z}^j) = \frac{\sum_{l=0}^{M^j - 1} (C^j_k)^{(M^j - l - 1)}(0) (G^{1:S}_{k|k-1})^{(l+1)} (s^{1:S}_{k|k-1}[1 - p^j_D]) \sigma^j_l(Z^j_k - \{\boldsymbol{z}^j\})}{\sum_{i=0}^{M^j} (C^j_k)^{(M^j - i)}(0) (G^{1:S}_{k|k-1})^{(i)} (s^{1:S}_{k|k-1}[1 - p^j_D]) \sigma^j_i(Z^j_k)}, \tag{20}$$

$$\sigma^j_i(Z^j_k) = \sigma_{M^j, i} \left(\frac{s^{1:S}_{k|k-1}[p^j_D L^j_{\boldsymbol{z}^j_1}]}{c^j_k(\boldsymbol{z}^j_1)}, \ldots, \frac{s^{1:S}_{k|k-1}[p^j_D L^j_{\boldsymbol{z}^j_{M^j}}]}{c^j_k(\boldsymbol{z}^j_{M^j})} \right), \tag{21}$$

where $p^j_D(\boldsymbol{x}, \boldsymbol{b})$ is the detection probability of the jth sensor, and $\sigma_{m,i}(y_1, \ldots, y_m)$ is the elementary symmetric function of degree i in $y_1, \ldots, y_m$ [6].

The maximum a posteriori (MAP) estimate of target number is

$$\hat{N}_{k|k} = \arg\sup_n p^{1:S}_{k|k}(n). \tag{22}$$

By looking for the $\hat{N}_{k|k}$ large local maxima of the extended PHD, the estimates of the multi-target states are derived as $\hat{X}_{k|k} = \{\hat{\boldsymbol{x}}_{k|k,n}\}_{n=1}^{\hat{N}_{k|k}}$. Since the sensor bias is the same for all targets, the estimate of the bias at time k is derived by

$$\hat{\boldsymbol{b}}_{k|k} = \frac{\int \boldsymbol{b}_k D^{1:S}_{k|k}(\boldsymbol{x}_k, \boldsymbol{b}_k) \mathrm{d}\boldsymbol{x}_k \mathrm{d}\boldsymbol{b}_k}{\hat{N}_{k|k}}. \tag{23}$$

4 Simulations

4.1 Example 1

Consider two two-dimensional scenarios with an unknown and time varying number of targets over the surveillance region $A = [-1000 \quad 1000] \times [-1000 \quad 1000]$ m^2 for a period of T =60 s. The targets are observed by multiple dissimilar but synchronous sensors. The sampling interval of the sensors is Δt=1 s. At time k, let N_k denote the actual target number, and $\boldsymbol{x}_{k,n} = [x_{k,n}, y_{k,n}, \dot{x}_{k,n}, \dot{y}_{k,n}, \ddot{x}_{k,n}, \ddot{y}_{k,n}]^{\mathrm{T}}$ denote the state vector of the nth ($n = 1, \ldots, N_k$) target.

Assume that the process noise $\boldsymbol{w}_{k,n}$ of the nth target is i.i.d zero-mean Gaussian white noise with the covariance matrix $\boldsymbol{Q}_{k,n}$. Then the Markovian transition probability density of $\boldsymbol{x}_{k,n}$ could be modeled as

$$f_{x,k|k-1}(\boldsymbol{x}_{k,n}|\boldsymbol{x}_{k-1,n}) = \mathcal{N}(\boldsymbol{x}_{k,n}|\boldsymbol{\Phi}_{k,n}\boldsymbol{x}_{k-1,n}, \boldsymbol{Q}_{k,n}), \tag{24}$$

where $\boldsymbol{\Phi}_{k,n}$ is discrete-time evolution matrix. Here $\boldsymbol{\Phi}_{k,n}$ and $\boldsymbol{Q}_{k,n}$ are given by the constant acceleration model [1]

$$\boldsymbol{\Phi}_{k,n} = \begin{bmatrix} 1 & \Delta t & \frac{\Delta t^2}{2} \\ & 1 & \Delta t \\ & & 1 \end{bmatrix} \otimes \boldsymbol{I}_2; \quad \boldsymbol{Q}_{k,n} = \sigma_w^2 \begin{bmatrix} \frac{\Delta t^4}{4} & \frac{\Delta t^3}{2} & \frac{\Delta t^2}{2} \\ \frac{\Delta t^3}{2} & \frac{\Delta t^2}{2} & \Delta t \\ \frac{\Delta t^2}{2} & \Delta t & 1 \end{bmatrix} \otimes \boldsymbol{I}_2; \quad \boldsymbol{I}_2 = \begin{bmatrix} 1 & \\ & 1 \end{bmatrix}, \tag{25}$$

where '$\otimes$' denotes the Kronecker product. The parameter σ_w is the instantaneous standard deviation of the acceleration, given by σ_w =0.05 m/s^2.

The number of the sensors over the region is $S = 3$. The range and bearing measurements of targets are generated by Sensor 1 located at $\boldsymbol{p}_k^1 = [p_x^1, p_y^1]^{\mathrm{T}}$. The range measurements of targets are generated by Sensor 2 located at $\boldsymbol{p}_k^2 = [p_x^2, p_y^2]^{\mathrm{T}}$. The bearing measurements of targets are generated by Sensor 3 located at $\boldsymbol{p}_k^3 = [p_x^3, p_y^3]^{\mathrm{T}}$. In this example, they are given by $\boldsymbol{p}_k^1 = [600, 400]^{\mathrm{T}}$ m, $\boldsymbol{p}_k^2 = [0, 0]^{\mathrm{T}}$ m and $\boldsymbol{p}_k^3 = [-600, -400]^{\mathrm{T}}$ m.

The measurement errors of the sensors consist of the translational measurement biases $\boldsymbol{b}_k^1 = [\Delta\rho_k^1, \Delta\theta_k^1]^{\mathrm{T}}$, $\boldsymbol{b}_k^2 = \Delta\rho_k^2$, $\boldsymbol{b}_k^3 = \Delta\theta_k^3$, and the random measurement noises $\boldsymbol{v}_k^1 = [\delta\rho_k^1, \delta\theta_k^1]^{\mathrm{T}}$, $\boldsymbol{v}_k^2 = \delta\rho_k^2$, $\boldsymbol{v}_k^3 = \delta\theta_k^3$. The dynamic model used for the bias $\boldsymbol{b}_k = [(\boldsymbol{b}_k^1)^{\mathrm{T}}, (\boldsymbol{b}_k^2)^{\mathrm{T}}, (\boldsymbol{b}_k^3)^{\mathrm{T}}]$ is a first-order Gauss-Markov process with the transition density given by [10]

$$f_{b,k|k-1}(\boldsymbol{b}_k|\boldsymbol{b}_{k-1}) = \mathcal{N}(\boldsymbol{b}_k^1|\beta^1\boldsymbol{b}_{k-1}^1, \boldsymbol{B}_{k-1}^1)\mathcal{N}(\boldsymbol{b}_k^2|\beta^2\boldsymbol{b}_{k-1}^2, \boldsymbol{B}_{k-1}^2)\mathcal{N}(\boldsymbol{b}_k^3|\beta^3\boldsymbol{b}_{k-1}^3, \boldsymbol{B}_{k-1}^3), \tag{26}$$

where β^j and $\boldsymbol{B}_k^j$ ($j = 1, 2, 3$) are, respectively, the discrete-time evolution parameter and the dynamics noise covariance for $\boldsymbol{b}_k^j$. For many real-world problems, the bias usually does not drift against time. So, we take $\beta^1 = \mathrm{diag}(1, 1)$, $\beta^2 = 1$, $\beta^3 = 1$ in this example. The biases and their covariances are given as $\boldsymbol{b}_k^1 = [50 \text{ m}, -50 \text{ mrad}]^{\mathrm{T}}$, $\boldsymbol{b}_k^2 = 30$ m, $\boldsymbol{b}_k^3 = -40$ mrad; $\boldsymbol{B}_k^1 = \mathrm{diag}((2.5 \text{ m})^2, (2.5 \text{ mrad})^2)$, $\boldsymbol{B}_k^2 = (2.5 \text{ m})^2$, $\boldsymbol{B}_k^3 = (2.5 \text{ mrad})^2$, where 'diag($\cdot$)' denotes diagonal matrix operation.

The random measurement noise $\boldsymbol{v}_k^j$ ($j = 1, 2, 3$) of the jth sensor is assumed to be i.i.d zero-mean Gaussian white noise with covariance matrix $\boldsymbol{R}_k^j$, which are given by $\boldsymbol{R}_k^1$= diag($(12.5 \text{ m})^2, (12.5 \text{ mrad})^2$), $\boldsymbol{R}_k^2$=(10 m)^2 and $\boldsymbol{R}_k^3$=(10 mrad)^2.

At time k, the likelihood $L_{\boldsymbol{z}_{k,m}^j}^j(\boldsymbol{x}_{k,n}, \boldsymbol{b}_k^j)$ of the jth sensor is given by

$$L_{\boldsymbol{z}_{k,m}^j}^j(\boldsymbol{x}_{k,n}, \boldsymbol{b}_k^j) = \mathcal{N}(\boldsymbol{z}_{k,m}^j|h_k^j(\boldsymbol{x}_{k,n}) + \boldsymbol{b}_k^j, \boldsymbol{R}_k^j), \tag{27}$$

where

$$\begin{cases} h_k^1(\boldsymbol{x}_{k,n}) = \begin{bmatrix} \sqrt{(x_{k,n} - p_x^1)^2 + (y_{k,n} - p_y^1)^2} \\ \arctan\frac{y_{k,n} - p_y^1}{x_{k,n} - p_x^1} \end{bmatrix}, \\ h_k^2(\boldsymbol{x}_{k,n}) = \sqrt{(x_{k,n} - p_x^2)^2 + (y_{k,n} - p_y^2)^2}, \\ h_k^3(\boldsymbol{x}_{k,n}) = \arctan\dfrac{y_{k,n} - p_y^3}{x_{k,n} - p_x^3}. \end{cases} \tag{28}$$

The detection probabilities of the sensors are $p^1_{D,k}(\boldsymbol{x}_k, \boldsymbol{b}^1_k) = 0.8$, $p^2_{D,k}(\boldsymbol{x}_k, \boldsymbol{b}^2_k) = 0.9$, $p^3_{D,k}(\boldsymbol{x}_k, \boldsymbol{b}^3_k) = 0.7$.

The clutter of the jth ($j = 1, 2, 3$) sensor is modeled as a Poisson RFS with intensity $\lambda^j_c c^j(\boldsymbol{z}^j_k)$, given as $\lambda^1_c = 60$, $\lambda^2_c = 50$, $\lambda^3_c = 40$, $c^1(\cdot) = c^2(\cdot) = c^3(\cdot) = \mathcal{U}(\cdot|A)$, where $\mathcal{U}(\cdot|A)$ denotes the probability density of the uniform distribution over the region A.

Figure 1 shows the true target trajectories and sensor locations in Scenario 1. In Figure 1, 'Δ' denotes the sensor location, '$\bigcirc$' denotes the locations at which the targets are born, '$\square$' denotes the locations at which the targets die and arrow denotes the direction of target motion. Target 1 is born at 1 s and dies at 40 s. Target 2 is born at 1 s and dies at 30 s. Target 3 is born at 15 s and dies at 50 s. Target 4 is born at 20 s and dies at 60 s.

The intensity of target birth at time k is modeled as

$$\gamma_k(\boldsymbol{x}_k) = \lambda_\gamma f_\gamma(\boldsymbol{x}_k|\psi_\gamma), \tag{29}$$

where λ_γ is the average number of the target birth per scan, $f_\gamma(\boldsymbol{x}_k|\psi_\gamma)$ is the probability density of the new born target's state, and ψ_γ is the set of the density parameters. In this example, they are taken as $\lambda_\gamma = 0.05$, $f_\gamma(\boldsymbol{x}_k|\psi_\gamma) = \pi^1_\gamma \mathcal{N}(\boldsymbol{x}_k|\boldsymbol{\mu}^1_\gamma, \boldsymbol{\Sigma}^1_\gamma) + \pi^2_\gamma \mathcal{N}(\boldsymbol{x}_k|\boldsymbol{\mu}^2_\gamma, \boldsymbol{\Sigma}^2_\gamma)$, where $\psi_\gamma = \{\pi^1_\gamma, \pi^2_\gamma, \boldsymbol{\mu}^1_\gamma, \boldsymbol{\mu}^2_\gamma, \boldsymbol{\Sigma}^1_\gamma, \boldsymbol{\Sigma}^2_\gamma\}$, $\pi^1_\gamma = \pi^2_\gamma = 0.5$, $\boldsymbol{\mu}^1_\gamma = [-600, 750, 0, 0, 0, 0]^{\mathrm{T}}$, $\boldsymbol{\mu}^2_\gamma = [-650, -800, 0, 0, 0, 0]^{\mathrm{T}}$ and $\boldsymbol{\Sigma}^1_\gamma = \boldsymbol{\Sigma}^2_\gamma = \mathrm{diag}(400, 400, 400, 400, 16, 16)$.

The probability of target survival is set at $p_{S,k|k-1}(\boldsymbol{x}_{k-1}) = 0.95$.

For the purpose of comparison, we estimate the translational measurement biases and the number and states of the targets, by using the extended multi-sensor PHD filter and the extended PM-CPHD filter, respectively. Both of the filters still involve multiple integrals. Thus they have no closed-form expressions in the non-linear and non-Gaussian conditions. The sequential Monte Carlo (SMC) method [11] can be used to implement the two filters. In the SMC implementations, 1000 particles are used to represent one surviving target and 500 particles are used to represent the new born targets. We now conduct MC simulation experiments on the same simulation setup except the independently generated clutter and target generated measurements.

The estimates of the translational measurement biases, derived by both methods at each time step, are shown along with the true biases in Figure 2.

Figure 2 shows that the bias estimates from the two methods converge to the ground truth after some time in this trial. Furthermore, the estimation accuracy of the extended PM-CPHD filter seems to be better than that of the extended multi-sensor PHD filter. In a few trials, some bias estimates from the two methods are inconsistent with the truth because of the effects of missing detections, clutter, random noise and so on. However, MC simulation results show that the bias estimates from the extended PM-CPHD filter can correctly converge in 98% of the trials while the extended multi-sensor PHD filter can correctly converge in 92% of the trials. The convergence time of the former is about 16–20 s while that of the latter is about 19–23 s.

The estimates of target positions, derived by both methods at each time step, are shown along with the true trajectories in Figures 3 and 4, respectively.

In Figures 3 and 4, '$\bigcirc$' denotes target position estimate, and the solid line denotes the actual target trajectory. From the figures, it can be seen that the position estimates of the extended PM-CPHD filter are closer to the ground truth than that of the extended multi-sensor PHD filter. That is because, as illustrated in Figure 2, the extended PM-CPHD filter can estimate and compensate for the translational measurement biases more accurately than the extended multi-sensor PHD filter.

The MC average of the means of the target number estimates, derived by both methods at each time step, along with the true target number is shown in Figure 5.

Figure 5 demonstrates the target number estimates derived by the two methods during the whole surveillance period. Since both filters can estimate and compensate for the translational measurement biases, their target number estimates are unbiased and close to the truth after the registration phase. On the other hand, the target number estimates from the extended PM-CPHD filter are more smooth and accurate than that of the extended multi-sensor PHD filter.

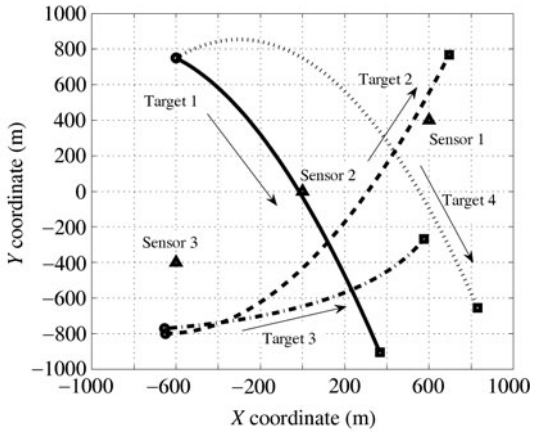

Figure 1 True target trajectories and sensor locations in Scenario 1.

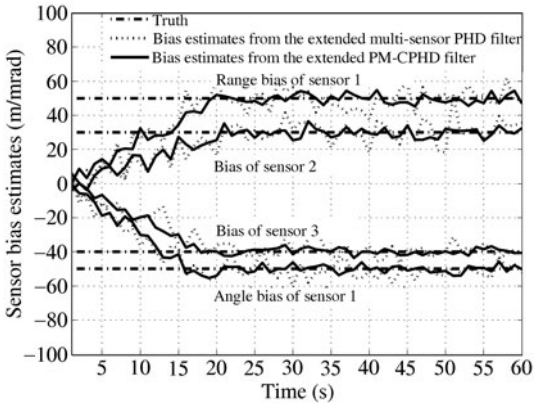

Figure 2 Estimates of the translational measurement biases from the two methods in one trial for Scenario 1.

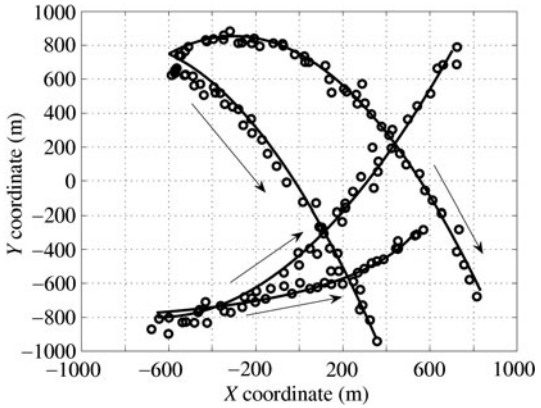

Figure 3 Estimates of target positions in one trial from the extended multi-sensor PHD filter for Scenario 1.

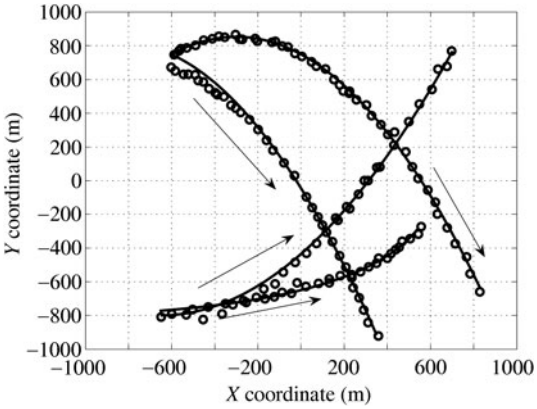

Figure 4 Estimates of target positions in one trial from the extended PM-CPHD filter for Scenario 1.

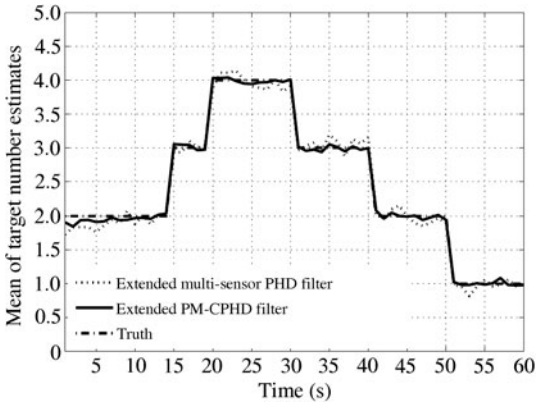

Figure 5 Hundred MC run average of the means of target number estimates against time for Scenario 1.

Two criteria, known as the optimal sub-pattern assignment (OSPA) metric and circular position error probability (CPEP) metric [12], are used to evaluate the performance of both methods.

Given the actual and estimated multi-target state sets $X_k = \{\boldsymbol{x}_{k,n}\}_{n=1}^{N_k}$ and $\hat{X}_{k|k} = \{\hat{\boldsymbol{x}}_{k|k,n}\}_{n=1}^{\hat{N}_{k|k}}$, the OSPA metric of order $p = 2$, with cut-off c between the two sets, is defined by

$$\mathrm{OSPA}_{2,k}^{(c)}(X_k, \hat{X}_{k|k}) = \left(\frac{1}{\hat{N}_{k|k}} \left(\min_{\pi \in \Pi_{\hat{N}_{k|k}}} \sum_{n=1}^{N_k} \min(c, ||\boldsymbol{x}_{k,n} - \hat{\boldsymbol{x}}_{k|k,\pi(n)}||_2)^2 + c^2(\hat{N}_{k|k} - N_k) \right) \right)^{1/2}, \quad (30)$$

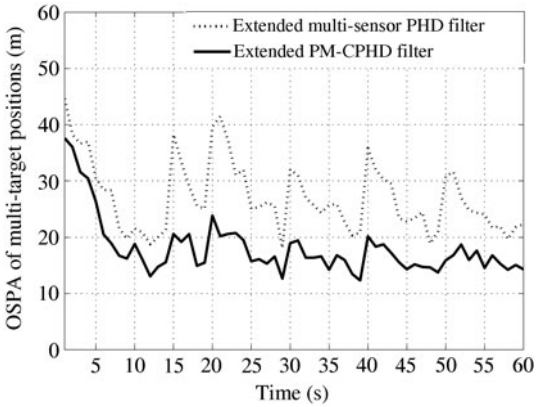

Figure 6 Hundred MC run average of OSPA against time for Scenario 1.

if $N_k \leqslant \hat{N}_{k|k}$ and $\mathrm{OSPA}_{2,k}^{(c)}(X_k, \hat{X}_{k|k}) = \mathrm{OSPA}_{2,k}^{(c)}(\hat{X}_{k|k}, X_k)$, if $N_k > \hat{N}_{k|k}$. $\Pi_{\hat{N}_{k|k}}$ denotes the set of permutations on $\{1, 2, \ldots, \hat{N}_{k|k}\}$. $||\cdot||_2$ denotes the 2-norm. In this example, we let c=80 m.

The MC averages of the OSPA metric for the target position estimates, derived by both methods, are shown at each time step in Figure 6.

The OSPA metric is composed of two components, each separately accounting for 'localization' and 'cardinality' errors. This results in high peaks in OSPA metric at the instances when the estimated number is incorrect. Figure 6 shows that the OSPA metric of the two methods becomes smaller and smaller during the registration phase. After the bias estimates converge, the OSPA metric of the extended PM-CPHD filter is smaller than that of the extended multi-sensor PHD filter. A reasonable explanation is that the former outperforms the latter in estimating both the target number and positions. Moreover, both curves in Figure 6 fluctuate against time because of the varying target number, the sensor-to-target geometry and clutter.

The CPEP metric at time k is defined by

$$\mathrm{CPEP}_k(r) = \frac{1}{N_k} \sum_{\boldsymbol{x}_k \in X_k} \mathrm{Prob}\{||\boldsymbol{H}_k \hat{\boldsymbol{x}}_{k|k} - \boldsymbol{H}_k \boldsymbol{x}_k||_2 > r, \forall \hat{\boldsymbol{x}}_{k|k} \in \hat{X}_{k|k}\};$$

$$\boldsymbol{H}_k = \begin{bmatrix} 1 & 0 & 0 & 0 & 0 & 0 \\ 0 & 1 & 0 & 0 & 0 & 0 \end{bmatrix}, \tag{31}$$

where r is a radius of CPEP metric. $\boldsymbol{H}_k \boldsymbol{x}_k$ and $\boldsymbol{H}_k \hat{\boldsymbol{x}}_{k|k}$, respectively, denote the actual and estimated target positions in a Cartesian coordinate. In this example, we let r=25 m.

The MC average of the CPEP metric for both methods at each time step is shown in Figure 7.

Differently from the OSPA metric, the CPEP metric only penalizes errors in individual state estimates but not errors in the estimated cardinality. Figure 8 demonstrates that the CPEP metric from the extended PM-CPHD filter is smaller than that of the extended multi-sensor PHD filter after registration phase. The reason for this phenomenon is that the estimates from the former are close to the ground truth and easily fall within a surrounding r= 25 m radius, whereas the estimates from the latter are relatively further away from the ground truth and easily go beyond the radius. Moreover, similar to the OSPA metric in Figure 6, the CPEP metric of the two methods becomes smaller and smaller during the registration phase. It implicitly reflects that the bias estimates are converging to the ground truth during the period.

The computational requirements for both methods are compared via the indication of CPU processing time. Based on MC runs, the average computational times per scan of a fairly optimal Matlab implementation for both algorithms on 1.83 GHz AMD Athlon (tm) XP 2500+ processor 512 MB RAM, are, respectively, 0.61 s and 2.88 s. It can be seen that the extended PM-CPHD filter is more computationally expensive than the extended multi-sensor PHD filter.

We consider Scenario 2 where multiple targets are traveling in parallel. Figure 8 shows the true target trajectories and sensor locations for the scenario. Targets 1 and 2 are born at 1 s and maintain a parallel

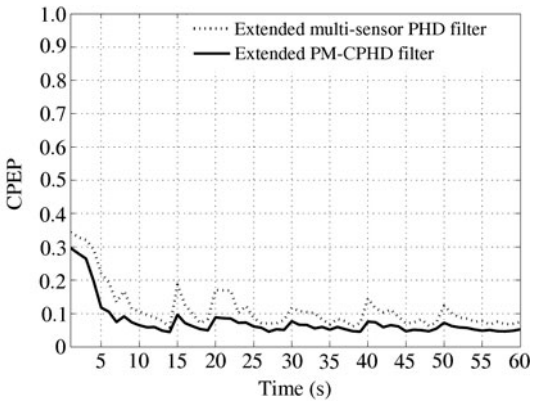

Figure 7 Hundred MC run average of CPEP against time for Scenario 1.

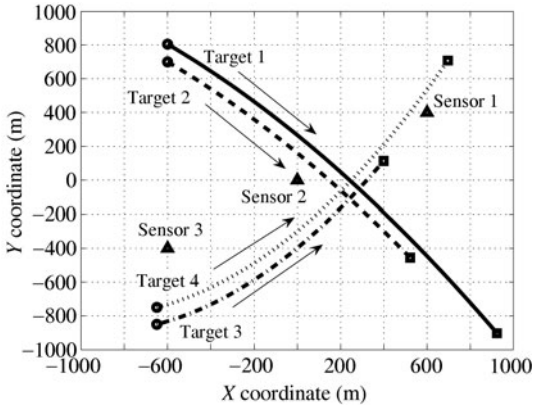

Figure 8 True target trajectories and sensor locations in Scenario 2.

movement until Target 1 dies at 40 s and Target 2 dies at 30 s. The distance between the parallel tracks of the two targets is about 100 m. Target 3 and 4 are born at 15 s and maintain a parallel movement until Target 3 dies at 50 s and Target 4 dies at 60 s. The distance between the parallel tracks of the two targets is about 90 m. The other simulation parameters are the same as those of Scenario 1.

In this scenario, since the distances between the parallel motion targets are very close, the complexity of joint spatial registration and MTT increases significantly compared with Scenario 1. For Scenario 2, MC simulation results show that the bias estimates from the extended PM-CPHD filter can correctly converge in 93% of the trials, while the extended multi-sensor PHD filter does this in 81% of the trials. The MC averages of the means of the target number estimates, the OSPA metric and the CPEP metric derived by both methods for Scenario 2 are shown in Figures 9–11, respectively.

As illustrated in Figures 9–11, the performance of the extended PM-CPHD filter degrades slightly, whereas the performance of the extended multi-sensor PHD filter degrades seriously. From Figure 9, it can be seen that the the means of target number estimates derived by the extended multi-sensor PHD filter fluctuate obviously against time. Correspondingly, the OSPA and CPEP from the extended multi-sensor PHD filter increase rapidly because of the inaccurate target number estimates. A possible explanation for this is that the approximation in the measurement-updated equation of the extended multi-sensor PHD filter would become imprecise when the targets are close together. Therefore, the extended PM-CPHD filter is more robust than the extended multi-sensor PHD filter for relatively complex multiple target motion scenarios.

4.2 Example 2

In this example, we evaluate the performance of the extended PM-CPHD filter by benchmarking it against the MSJPDA filter, which is a classical association-based multi-sensor filter for tracking a known number of targets in clutter. In the MSJPDA filter, $(\boldsymbol{x}_k, \boldsymbol{b}_k)$ is also treated as an augmented state for joint spatial registration and MTT. The MSJPDA is given the correct number of targets whereas the extended PM-CPHD filter has no knowledge of the number of targets. For convenience, we assume that the sensors have the same detection probabilities and clutter rates

$$p^1_{D,k}(\boldsymbol{x}_k, \boldsymbol{b}^1_k) = p^2_{D,k}(\boldsymbol{x}_k, \boldsymbol{b}^2_k) = p^3_{D,k}(\boldsymbol{x}_k, \boldsymbol{b}^3_k) = p_D; \quad \lambda^1_c = \lambda^2_c = \lambda^3_c = \lambda_c. \tag{32}$$

The other experiment settings are the same as those of Example 1.

Let the detection probabilities of the sensors be fixed at $p_D = 0.9$. We compare the tracking performance of the two algorithms for various clutter rates. Tables 1 and 2, respectively, show the time averaged OSPA and CPEP metrics in various λ_c for Scenarios 1 and 2.

From Tables 1 and 2, it can be seen that the MSJPDA filter outperforms the extended PM-CPHD filter when the λ_c is relatively low. A reason for this phenomenon is that the translational measurement mis-registration would not lead to a serious impairment of data association result in a relatively sparse

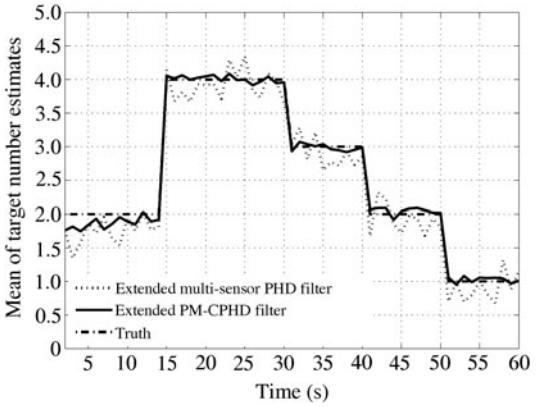

Figure 9 Hundred MC run average of the means of target number estimates against time for Scenario 2.

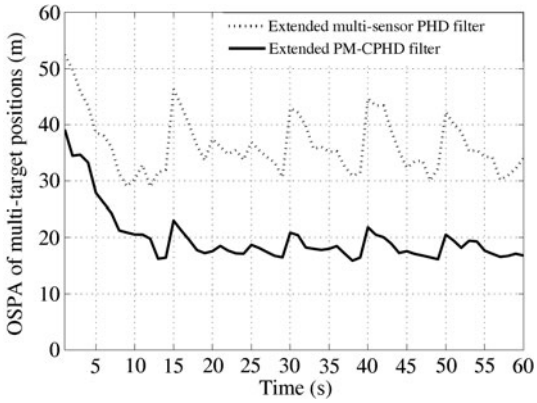

Figure 10 Hundred MC run average of OSPA against time for Scenario 2.

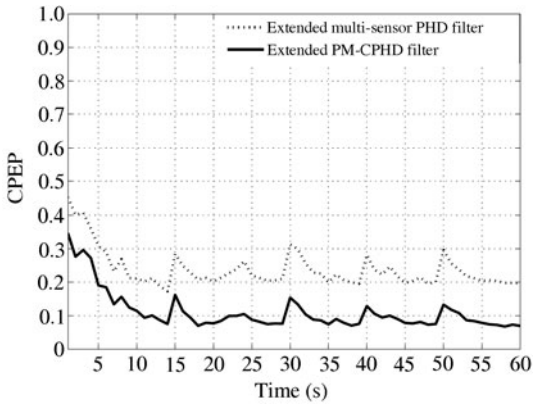

Figure 11 Hundred MC run average of CPEP against time for Scenario 2.

Table 1 Time averaged OSPA(m)/CPEP in various λ_c for Scenario 1

	λ_c=50	λ_c=100	λ_c=200	λ_c=300	λ_c=400	λ_c=500
Extended PM-CPHD filter	20.3/0.099	22.1/0.118	28.6/0.203	32.8/0.264	38.4/0.315	41.9/0.401
MSJPDA filter	15.6/0.086	19.1/0.107	27.7/0.196	37.2/0.289	49.1/0.432	63.8/0.603

Table 2 Time averaged OSPA(m)/CPEP in various λ_c for Scenario 2

	λ_c=50	λ_c=100	λ_c=200	λ_c=300	λ_c=400	λ_c=500
Extended PM-CPHD filter	22.3/0.119	24.8/0.146	30.7/0.268	36.7/0.335	42.3/0.409	49.1/0.481
MSJPDA filter	21.2/0.112	25.7/0.149	33.4/0.294	49.3/0.421	63.2/0.589	78.8/0.776

clutter environment. However, the performance of the MSJPDA filter degrades much more rapidly than that of the extended PM-CPHD filter as the λ_c increases, although the latter possibly has an additional error in the estimation of the target number. Furthermore, as the λ_c increases, the extended PM-CPHD filter exceeds the MSJPDA filter more rapidly in Scenario 2 than that in Scenario 1. A reasonable explanation is that when the clutter is relatively dense or the targets are relatively close, the data association becomes rather difficult because of the effect of the translational measurement misregistration. The possibly incorrect association would rapidly lead to the divergence of the bias and target state estimates. As a result, the association-based MSJPDA filter performs the joint spatial registration and MTT much worse than the extended PM-CPHD filter, when the λ_c is relatively high.

5 Conclusions and future work

An extended PM-CPHD filter is proposed for joint spatial registration and MTT. Simulation results show that the proposed method can estimate and compensate for the translational measurement biases more accurately. So, it outperforms the extended multi-sensor PHD filter in estimating the number and states of the targets. Moreover, it also outperforms the MSJPDA filter in a relatively dense clutter environment.

One of our future works will be focused on proposing an extended linear-complexity PM-CPHD filter [13] for joint spatial registration and MTT to reduce the computational cost of the new presented method.

Acknowledgements

This work was supported by National Natural Science Foundation of China (Grant Nos. 61004087, 61104214, 91016020, 61104051), China Postdoctoral Science Foundation (Grant Nos. 20100481338, 2011M501443), Fundamental Research Funds for the Central University and Doctoral Fund of Ministry of Education of China (Grant No. 20100201120036), Gansu Provincial Science and Technology Planning for China (Grant No. 0916RFZA017).

References

1 Dana M P. Multitarget Multisensor Tracking: Advanced Applications. MA: Artech House Publisher, 1990. 155–185
2 Herrero J G, Portas J, Corredera J. On-line multi-sensor registration for data fusion on airport surface. IEEE Trans Aerosp Electron Syst, 2007, 43: 356–370
3 Bar-Shalom Y, Li X R. Multitarget Multisensor Tracking: Principles and Techniques. Storrs: YBS Publishing, 1995
4 Wang M H, Wan Q, You Z S. A gate size estimation algorithm for data association filters. Sci China Ser F-Inf Sci, 2008, 51: 70–83
5 Mahler R. Multi-target Bayes filtering via first-order multi-target moments. IEEE Trans Aerosp Electron Syst, 2003, 39: 1152–1178
6 Mahler R. PHD filters of higher order in target number. IEEE Trans Aerosp Electron Syst, 2007, 43: 1523–1543
7 Lian F, Han C Z, Liu W F, et al. Joint spatial registration and multi-target tracking using an extended probability hypothesis density filter. IET Radar Sonar Navig, 2011, 5: 441–448
8 Mahler R. Approximate multisensor CPHD and PHD filters. In: Proceedings of the 13th International Conference on Information Fusion, Edinburgh, 2010. 1–8
9 Pao L Y, Frei C W. A comparison of parallel and sequential implementation of a multisensor multitarget tracking algorithm. In: Proceedings of the 1995 American Control Conference Seattle, Washington, 1995. 1683–1687
10 Kastella K, Yeary B, Zadra T, et al. Bias modeling and estimation for GMTI applications. In: Proceedings of the 3rd International Conference on Information Fusion, Paris, 2000. 1–8
11 Vo B N, Singh S, Doucet A. Sequential Monte Carlo methods for multi-target filtering with random finite sets. IEEE Trans Aerosp Electron Syst, 2005, 41: 1224–1245
12 Schuhmacher D, Vo B T, Vo B N. A consistent metric for performance evaluation of multi-object filters. IEEE Trans Signal Process, 2008, 86: 3447–3457
13 Mahler R. Linear-complexity CPHD filters. In: Proceedings of the 13th International Conferece on Information Fusion, Edinburgh, 2010. 1–8